Acta Crystallographica Section D
Biological Crystallography
ISSN 1399-0047

Structural and thermodynamic basis of the inhibition of *Leishmania major* farnesyl diphosphate synthase by nitrogen-containing bisphosphonates

Srinivas Aripirala,[a] Dolores Gonzalez-Pacanowska,[b] Eric Oldfield,[c] Marcel Kaiser,[d] L. Mario Amzel[e]* and Sandra B. Gabelli[e,f]*

[a]Institute for Multiscale Modeling of Biological Interactions and Department of Biophysics and Biophysical Chemistry, Johns Hopkins University, 725 North Wolfe Street WBSB 605, Baltimore, MD 21210, USA, [b]López-Neyra Institute of Parasitology and Biomedicine, 18001 Granada, Spain, [c]Department of Chemistry, University of Illinois at Urbana-Champaign, Urbana, IL 61801, USA, [d]University of Basel, Petersplatz 1, CH-4003 Basel, Switzerland, [e]Department of Biophysics and Biophysical Chemistry, Johns Hopkins University School of Medicine, 725 N. Wolfe Street WBSB 604, Baltimore, MD 21205, USA, and [f]Departments of Medicine and Oncology, Johns Hopkins University School of Medicine, Baltimore, MD 21205, USA

Correspondence e-mail: mamzel@jhmi.edu, gabelli@jhmi.edu

Received 31 October 2013
Accepted 8 December 2013

PDB references: LmFPPS, complex with 300B, IPP and Ca^{2+}, 4jzb; complex with 476A, IPP and Ca^{2+}, 4jzx; complex with 46I and Mg^{2+}, 4k10

Farnesyl diphosphate synthase (FPPS) is an essential enzyme involved in the biosynthesis of sterols (cholesterol in humans and ergosterol in yeasts, fungi and trypanosomatid parasites) as well as in protein prenylation. It is inhibited by bisphosphonates, a class of drugs used in humans to treat diverse bone-related diseases. The development of bisphosphonates as antiparasitic compounds targeting ergosterol biosynthesis has become an important route for therapeutic intervention. Here, the X-ray crystallographic structures of complexes of FPPS from *Leishmania major* (the causative agent of cutaneous leishmaniasis) with three bisphosphonates determined at resolutions of 1.8, 1.9 and 2.3 Å are reported. Two of the inhibitors, 1-(2-hydroxy-2,2-diphosphonoethyl)-3-phenylpyridinium (300B) and 3-butyl-1-(2,2-diphosphonoethyl)pyridinium (476A), co-crystallize with the homoallylic substrate isopentenyl diphosphate (IPP) and three Ca^{2+} ions. A t hird inhibitor, 3-fluoro-1-(2-hydroxy-2,2-diphosphonoethyl)-pyridinium (46I), was found to bind two Mg^{2+} ions but not IPP. Calorimetric studies showed that binding of the inhibitors is entropically driven. Comparison of the structures of *L. major* FPPS (LmFPPS) and human FPPS provides new information for the design of bisphosphonates that will be more specific for inhibition of LmFPPS. The asymmetric structure of the LmFPPS–46I homodimer indicates that binding of the allylic substrate to both monomers of the dimer results in an asymmetric dimer with one open and one closed homoallylic site. It is proposed that IPP first binds to the open site, which then closes, opening the site on the other monomer, which closes after binding the second IPP, leading to the symmetric fully occupied FPPS dimer observed in other structures.

1. Introduction

Leishmaniasis, a parasitic disease caused by any one of the 20 species of eukaryotic organisms of the genus *Leishmania*, is transmitted by the bite of female phlebotomine sand flies. The disease exists in three forms: cutaneous leishmaniasis (CL), visceral leishmaniasis (VL) and mucocutaneous leishmaniasis (ML). The World Health Organization has reported that leishmaniasis is endemic in 88 countries and threatens 350 million people (World Health Organization, 2014). CL, caused by *L. major* and *L. mexicana*, is predominantly found in Saudi Arabia, Iran, Afghanistan, Pakistan, Peru and Brazil, where it affects 12 million people, with 1.5 million new cases being reported annually. VL, caused by *L. donovani* and *L. infantum*, affects people in Bangladesh, India, Nepal, Sudan and Brazil. ML, caused primarily by *Leishmania braziliensis*, is found in Bolivia, Peru, Paraguay, Ecuador, Colombia and Venezuela.

Drugs that are presently used for the treatment of leishmaniasis include amphotericin B, ketoconazole, miltefosine,

Table 1
Structures of LmFPPS complexes: data-collection and refinement statistics.

Values in parentheses are for the highest resolution shell.

	LmFPPS–476A–IPP–Ca^{2+}	LmFPPS–300B–IPP–Ca^{2+}	LmFPPS–46I–Mg^{2+}
Space group	$P2_12_12_1$	$P2_12_12_1$	$P2_12_12_1$
Unit-cell parameters (Å, °)	a = 80.3, b = 85.7, c = 106.7, $\alpha = \beta = \gamma$ = 90	a = 80.4, b = 86.0, c = 107.1, $\alpha = \beta = \gamma$ = 90	a = 60.2, b = 143.7, c = 194.3, $\alpha = \beta = \gamma$ = 90
X-ray source/detector	FR-E/R-AXIS IV	FR-E/R-AXIS IV	Beamline 31-ID, APS
Resolution (Å)	50.0–1.8 (1.86–1.80)	50.0–1.9 (1.97–1.90)	50.0–2.3 (2.38–2.30)
Measured reflections	469090	400007	384740
Unique reflections	68699	58810	69237
$\langle I/\sigma(I)\rangle$	36.6 (2.4)	32.5 (2.9)	34.25 (3.3)
Completeness (%)	99.8 (99.9)	99.4 (95.3)	91.2 (96.5)
R_{merge} (%)	7.0 (54.5)	7.2 (47.3)	10.6 (67.5)
Refinement			
R_{cryst} (%)	17.8	17.2	22.7
R_{free} (%)	22.9	21.3	28.4
Monomers in asymmetric unit	2	2	4
No. of protein atoms	5786	5808	11474
No. of water molecules	693	678	294
R.m.s. deviations			
Bond lengths (Å)	0.008	0.010	0.009
Angles (°)	1.1	1.2	1.6
B factors (Å^2)			
Protein	26.7	22.0	45.5
Ligand	25.2	19.7	73.8
Water	36.5	31.9	42.4

paromomycin and pentamidine, in addition to the antimony-containing compounds meglumine antimoniate and sodium stibogluconate. However, most require long treatments, have serious side effects and are too expensive. The shortcomings of these drugs point to a critical need to find new therapeutic compounds.

Bisphosphonates such as pamidronate and risedronate, drugs that are used in humans for the treatment of osteoporosis (Rodan & Martin, 2000; Reszka *et al.*, 1999), are effective against the *Leishmania* parasite both *in vitro* and *in vivo* (Sanders *et al.*, 2005; Rodriguez *et al.*, 2002). These bisphosphonates target farnesyl diphosphate synthase (FPPS), a key enzyme in mevalonate/isoprenoid biosynthesis (Reszka *et al.*, 1999). FPPS catalyzes both the 1′–4 condensation of two five-carbon compounds (C-5), isopentenyl diphosphate (IPP) and its isomer dimethylallyl diphosphate (DMAPP), to produce geranyl diphosphate (GPP; C-10), and the subsequent condensation of GPP with IPP to produce farnesyl diphosphate (FPP; C-15). In eukaryotes, FPP is a main branch point of the mevalonate pathway. It is the substrate of squalene synthase, which leads to the production of sterols and also of farnesyl transferase, which leads to the prenylation of proteins such as Ras, lamin A and others that contain a CAAX box at the C-terminus. In addition, FPP is a precursor to dolichols, compounds that are essential in the N-glycosylation of proteins.

Bisphosphonates are ideal candidates for the development of new, more effective drugs against *Leishmania* parasites because of their proven safety in humans. Since the sequence identity among the FPPS of *L. major*, *L. infantum*, *L. donovani* and *L. mexicana* is greater than 90%, it may be possible to design compounds that inhibit this enzyme in all *Leishmania* strains (Supplementary Fig. S1[1]). In this paper, we report the thermodynamic data for the binding of four nitrogen-containing bisphosphonate inhibitors (Fig. 1) to *L. major* FPPS (LmFPPS), as well as the structures of three of these complexes. The structures show that while LmFPPS is structurally similar to human FPPS, differences in the catalytic pocket identified in this work should open the way for the design of parasite-specific inhibitors. The thermodynamic footprint of binding of these inhibitors to LmFPPS, determined by isothermal titration calorimetry (ITC), provides additional clues for inhibitor design. In addition, the structure of the complex of LmFPPS with the bisphosphonate 3-fluoro-1-(2-hydroxy-2,2-diphosphonoethyl)pyridinium (46I) provides structural insights into the ordered sequential mechanism proposed by Laskovics & Poulter (1981). In this structure with the two allylic sites occupied, the two empty IPP sites adopt different conformations, one open and one closed, suggesting an alternating-site mechanism for binding of the homoallylic substrate.

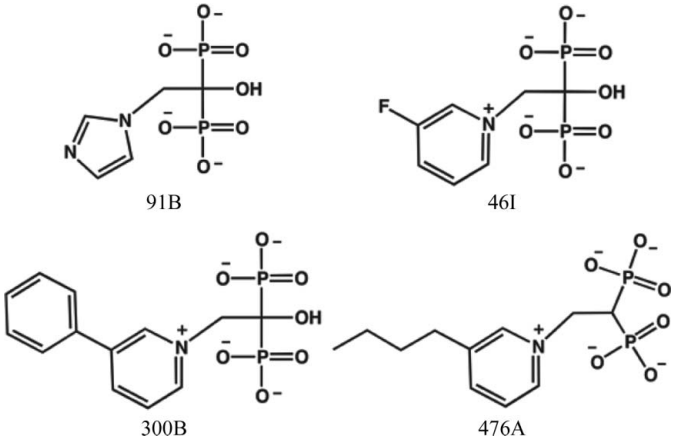

Figure 1
The bisphosphonates used in this study.

2. Materials and methods

2.1. Synthesis of bisphosphonates

The bisphosphonate inhibitors 1-(2-hydroxy-2,2-diphosphonoethyl)-3-phenylpyridinium (300B), 3-fluoro-1-(2-hydroxy-2,2-diphosphonoethyl)pyridinium (46I) and 476A (CAS Registry No. 882569-40-6) were synthesized as reported previously (Sanders *et al.*, 2005; Zhang *et al.*, 2006). These

[1] Supporting information has been deposited in the IUCr electronic archive (Reference: DW5084).

inhibitors were chosen based on their strong binding affinity (nanomolar K_d) towards *Trypanosoma cruzi* FPPS (Huang *et al.*, 2010). Their ability to be modified and tailored to bind *Leishmania* FPPS according to the results of this study was also a consideration.

2.2. Cloning, expression and purification

LmFPPS was cloned and expressed as reported previously (Ortiz-Gómez *et al.*, 2006). Briefly, DNA coding for LmFPPS (with an N-terminal His tag and thrombin cleavage site) was cloned into pET-28a vector (Novagen). *Escherichia coli* BL21 (DE3) cells transformed with this plasmid were grown in LB medium until they reached an OD_{600} of 0.8 and were induced with 0.1 m*M* IPTG at 37°C. Cells were harvested 3 h after induction and were washed in buffer *A* (50 m*M* NaH_2PO_4 pH 8.0, 300 m*M* NaCl, 10 m*M* imidazole, 1 m*M* TCEP). The cells were broken with a microfluidizer, the lysate was centrifuged for 30 min at 12 000 rev min^{-1} and the supernatant was loaded onto a HisTrap Ni^{2+}-chelate affinity column equilibrated with buffer *A*. Protein was eluted using a linear gradient of 0–100% buffer *B* (50 m*M* NaH_2PO_4 pH 8.0, 300 m*M* NaCl, 500 m*M* imidazole, 1 m*M* TCEP). After cleaving the polyhistidine tag by digestion with thrombin, the sample was loaded onto an anion-exchange column (binding buffer: 20 m*M* Tris pH 8.2, 50 m*M* NaCl, 1 m*M* TCEP) and eluted with 20 m*M* Tris pH 8.2, 1 *M* NaCl, 1 m*M* TCEP. The eluate was further purified using a second round of nickel-affinity chromatography, collecting the flowthrough. The protein was dialyzed against 20 m*M* Tris pH 8.2, 150 m*M* NaCl, 1 m*M* TCEP and concentrated to 15 mg ml^{-1}.

2.3. Crystallization

After identifying crystallization conditions using an incomplete factorial set with 600 nl hanging drops (Jancarik & Kim, 1991), crystals for data collection were grown by vapour diffusion using a 1:1 ratio of the protein and reservoir (15–25% PEG 3350, 0.1–0.2 *M* calcium acetate, 0.1 *M* MES sodium salt pH 6.5) solutions. Protein–inhibitor complexes were co-crystallized from solutions consisting of 12.5 mg ml^{-1} LmFPPS, 250 µ*M* inhibitor, 250 µ*M* IPP and 1 m*M* $MgCl_2$. Crystals belonging to the orthorhombic space group $P2_12_12_1$ appeared within 1–2 d. The crystals of the 300B and 476A complexes had the same unit-cell parameters, but the unit cell of the 46I complex was significantly larger (Table 1).

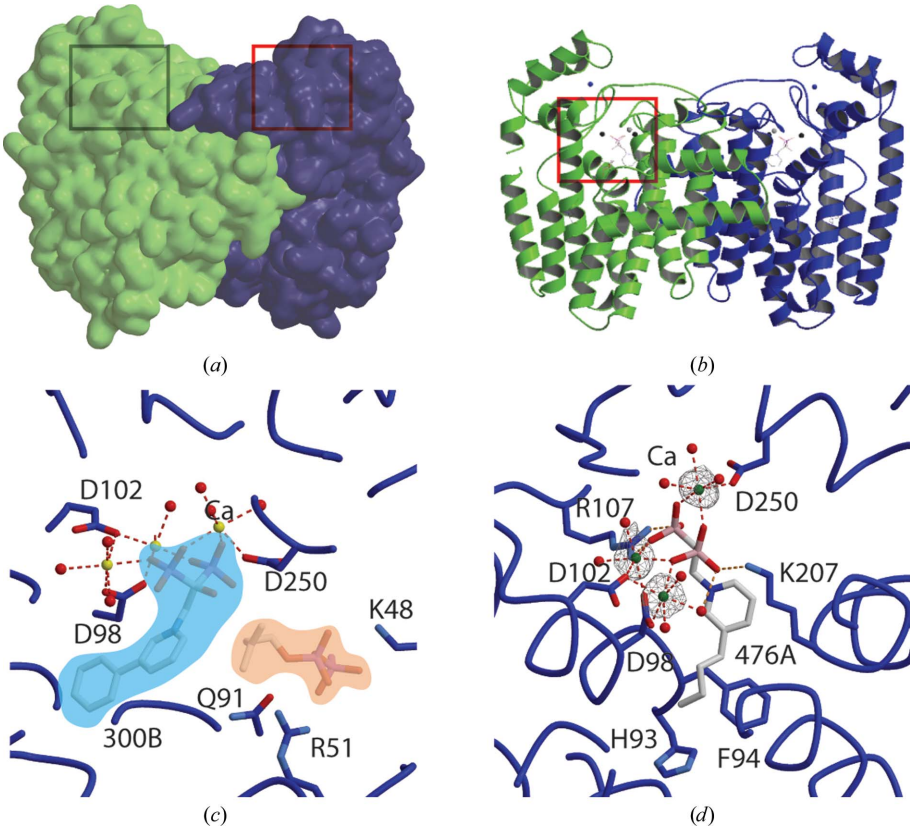

Figure 2
Dimer of LmFPPS. (*a*) Surface representation of the complex with 300B, IPP and three divalent cations. The two boxes show the active site in each of the two monomers. (*b*) Ribbon representation of the complex. 300B and IPP are shown as stick models, while the divalent cations (Ca^{2+}) are shown as spheres. The box shows the active site in one of the monomers. (*c*) Octahedral coordination of the Ca^{2+} is shown as red dashed lines. Water molecules are shown as red spheres and Ca^{2+} ions as yellow spheres. Protein backbone and the residues in the active site are shown in blue. 300B and IPP are shown as a stick models in white. The blue shaded region highlights the allylic site, while the homoallylic site is shown as an orange shaded region. (*d*) LmFPPS in complex with 476A, IPP and three Ca^{2+} ions. The divalent cations were determined to be Ca^{2+} using anomalous scattering data measured at the wavelength corresponding to the Cu edge. Water molecules are shown as red spheres and Ca^{2+} ions are shown in green. Protein backbone and the residues in the active site are shown in blue. 476A is shown as a stick model in white. Residues from the first and second aspartate-rich regions are shown coordinating Ca^{2+} ions. The density shown around the Ca^{2+} ions was calculated using anomalous scattering data.

2.4. Data collection

Crystals cryoprotected in mother liquor were flash-cooled at 100 K. Diffraction data for the 300B and 476A complexes were collected in-house using an FR-E X-ray source with an R-AXIS IV detector, while data for the LmFPPS–46I–Mg complex were collected on beamline 31-ID of the Advanced Photon Source (APS). Data were processed and scaled with the *HKL*-2000 suite (Otwinowski & Minor, 1997; Table 1).

2.5. Structure determination and refinement

The LmFPPS structure was determined by molecular replacement with *AMoRe* (Navaza, 1994) using the coordinates of the FPPS from *T. cruzi* (PDB entry 1yhk; 60% sequence identity; Gabelli *et al.*, 2006) as the search model.

After changing the sequence to that of LmFPPS with the program *O* (Jones *et al.*, 1991), iterative cycles of refinement and rebuilding were carried out with *REFMAC*5 (Winn *et al.*, 2001, 2011; Murshudov *et al.*, 2011) and *Coot* (Emsley *et al.*, 2010). The progress of the refinement was monitored by following the *R* value and the R_{free} value (calculated using 5% of the reflections). The overall quality of the final model was assessed using *PROCHECK* (Laskowski *et al.*, 1993) and *WHAT IF* (Hooft, Vriend *et al.*, 1996; Hooft, Sander *et al.*, 1996). Visualization, analysis and figure preparation were carried out with *MolScript* (Kraulis, 1991) and *PyMOL* (v.1.5.0.1; Schrödinger). The calculation of the buried area upon dimer formation was carried out using *AREAIMOL* in the *CCP*4 suite (Lee & Richards, 1971). The identity of the cation in the LmFPPS–300B–IPP and LmFPPS–476A–IPP structures was determined by calculating an anomalous map with data collected at the Cu *Kα* wavelength and verifying that the coordination had the correct distances and numbers of ligands. In the case of LmFPPS–46I the identity of the cations could not be verified by anomalous scattering data since neither Ca^{2+} nor Mg^{2+} (both possible candidates) has anomalous signal at the wavelength at which the data were collected (λ = 0.979 Å); however, the coordination and bond distances strongly suggest the presence of Mg^{2+}

2.6. Isothermal titration calorimetry

The binding of LmFPPS to four ligands, 1-(2-hydroxy-2,2-diphosphonoethyl)-3-phenylpyridinium (300B), 3-butyl-1-(2,2-diphosphonoethyl)pyridinium (476A), 3-fluoro-1-(2-hydroxy-2,2-diphosphonoethyl)pyridinium (46I) and 1-hydroxy-2-imidazolyl-ethylidene-1,1-bisphosphonate monohydrate (91B; zoledronate; Huang *et al.*), was studied by isothermal titration calorimetry using a VP-ITC instrument (MicroCal Inc., Northampton, Massachusetts, USA). For these experiments the protein was diluted to 25 µ*M* (based on monomer molecular weight) in a buffer consisting of 25 m*M* HEPES pH 7.5, 1 m*M* TCEP, 300 m*M* NaCl, 5 m*M* $MgCl_2$. Ligand solutions were prepared in the same buffer at a concentration of 250 µ*M*. 1.4 ml of protein solution in the sample cell was titrated with 24 10 µl injections after an initial 2 µl injection. The heat evolved at 28°C after each ligand injection was obtained by integration of the calorimetric signal after subtracting the average heat of dilution. The data were analysed with the *Origin* 5.0 software and fitted using a one binding site per monomer model.

3. Results and discussion

3.1. Overall structure of LmFPPS complexes

The structures of the complexes of LmFPPS with the three bisphosphonate inhibitors 300B, 476A and 46I were determined by X-ray diffraction at resolutions of 1.8, 1.9 and 2.3 Å, respectively. The structures of the 300B and 476A complexes also contained the homoallylic substrate IPP and three Ca^{2+} ions, while that of the 46I complex contained two Mg^{2+} ions but no IPP (Table 1). LmFPPS is a homodimer similar to those of FPPS from other species (Gabelli *et al.*, 2006; Rondeau *et al.*, 2006; Tarshis *et al.*, 1994; Figs. 2*a* and 2*b*). The formation of the dimer buries 5770 $Å^2$ of accessible surface area. The

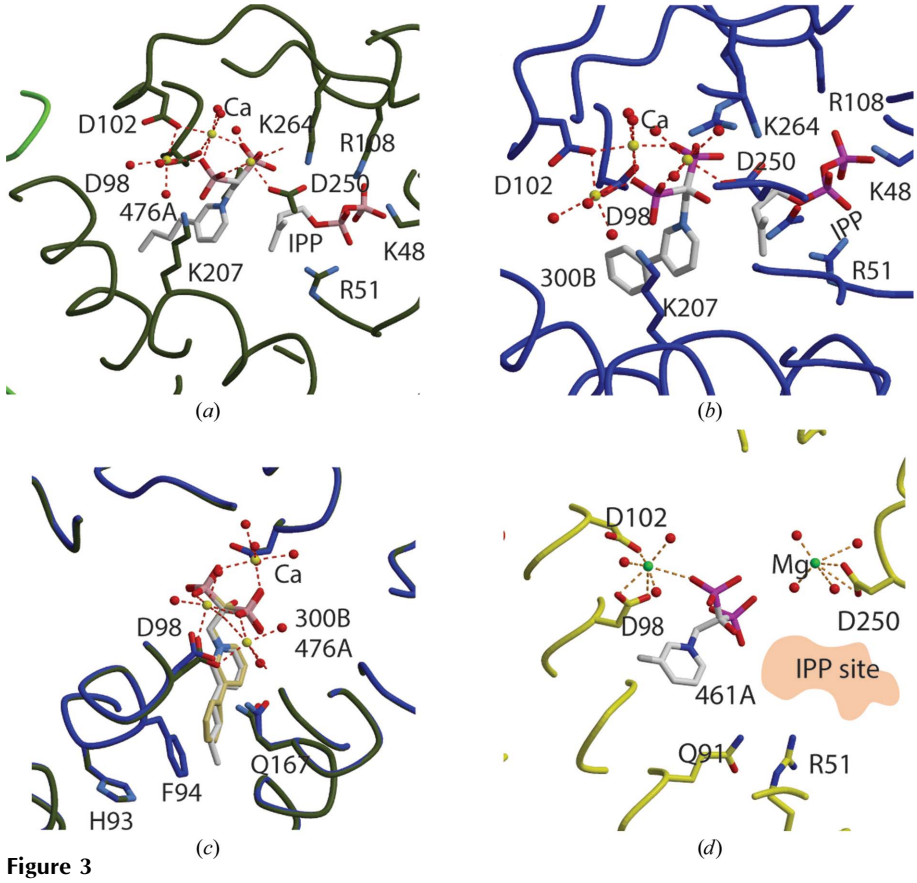

Figure 3
Active site of LmFPPS in complex with bisphosphonates. (*a*) LmFPPS in complex with 476A, IPP and three divalent cations. Water molecules are shown as red spheres and Ca^{2+} ions in yellow. Protein backbone and the residues in the active site are shown in dark green. 476A and IPP are shown in white as stick models. Residues from the first and second aspartate-rich motifs are shown coordinating Ca^{2+}. The basic amino acids Arg108, Arg51 and Lys48 are observed interacting with the diphosphate moiety of IPP. (*b*) Active site of LmFPPS in complex with 300B (white, stick representation), three Ca^{2+} ions (yellow, spheres) and IPP (white, stick representation) shown in the same orientation as in (*a*). (*c*) Structural alignment of the LmFPPS–300B–IPP–Ca complex (green) with the LmFPPS–476A–IPP–Ca complex (blue). Residues Asp98, Asp102 and Asp250 that participate in the ion/bisphosphonate coordination overlapped without any conformational differences. Gln167 (red arrow) in the 300B complex (blue) rotates 20° (χ_2) to accommodate the bulkier ligand 300B. (*d*) Active site of LmFPPS in complex with 46I (white, stick model) and two Mg^{2+} ions (green spheres) shown in the same orientation as in (*a*). The orange shaded region shows the empty IPP site.

monomers have the typical FPPS fold: a ten-helix bundle with four additional helices running perpendicular to the bundle. The two substrate sites, allylic and homoallylic, are part of a large connected cavity at the 'top' of the helix bundle. In the structures of the complexes, the inhibitors occupy the allylic site and IPP (when present) occupies the homoallylic site (Fig. 2*c*). Three divalent cations and the side chains of aspartate residues from two aspartate-rich motifs (DD*XX*D; residues 98–102 in the first aspartate-rich and residues 250–254 in the second aspartate-rich motif) coordinate the bisphosphonate atoms of the inhibitors bound at the allylic site (Gabelli *et al.*, 2006; Tarshis *et al.*, 1996; Kavanagh *et al.*, 2006). The divalent cations at the active site are octahedrally coordinated by water molecules and the O atoms of the bisphosphonates (Gabelli *et al.*, 2006; Tarshis *et al.*, 1996; Kavanagh *et al.*, 2006). In the structures reported here, the three divalent cations in the structures of LmFPPS–300B–IPP and LmFPPS–476A–IPP were determined to be Ca^{2+} using anomalous scattering data (Fig. 2*d*). Although Mg^{2+} is probably the physiological cation (Tarshis *et al.*, 1996), Ca^{2+} from the crystallization solution is present in these crystals.

3.2. Interactions of 300B and 476A with LmFPPS

The bisphosphonate moieties of both 300B and 476A interact with residues in the active site in a similar manner (Figs. 3*a* and 3*b*). Their phosphonate moieties accept hydrogen bonds from the amino groups of Lys207 and Lys264 and the guanidinium of Arg107 and interact indirectly through Ca^{2+} ions or water molecules with the carboxylates of Asp98, Asp102 and Asp250. The carboxylate of Asp99, which is at hydrogen-bonding distances from the N^{ε} and $N^{\eta 2}$ atoms of Arg107, positions Arg107 to interact with the phosphate of the inhibitor. Deeper in the active site, Leu95, Met101 and Phe94 interact with either the alkyl chain of 476A or the benzene ring of 300B. The side chain of Gln167, at the end of the active site, is in a different conformation in the two structures: it rotates by approximately 20° (χ_2) to accommodate 300B, the bulkier ligand (Fig. 3*c*). His93, which is thought to be involved in determining the product length (Ohnuma *et al.*, 1996), is in the same conformation in both complexes (Fig. 3*c*).

The hydroxyl group at the C1 position of 300B makes a hydrogen bond to Asp250 (distance of 2.9 Å). In contrast to the structure of *T. cruzi* FPPS, in which the presence of the C1 OH causes disordering of IPP in the active site (Huang *et al.*), the IPP in the structure of LmFPPS with 300B is well ordered (average temperature factor of 21.75 Å^2).

3.3. Interaction of 46I with LmFPPS

Although the complex of LmFPPS with 46I crystallizes in the same $P2_12_12_1$ space group as the other two complexes, its crystals are not isomorphous with the others. Unlike the structures of the complexes with 300B and 476A, which have one dimer in the asymmetric unit, the asymmetric unit of the 46I complex contains two dimers. Surprisingly, even though IPP was present in the crystallization buffer, there was no density for IPP in the active sites of any of the four monomers (Fig. 3*d*). Neither sulfate nor phosphate was observed to occupy the position of IPP; these ions have been observed to

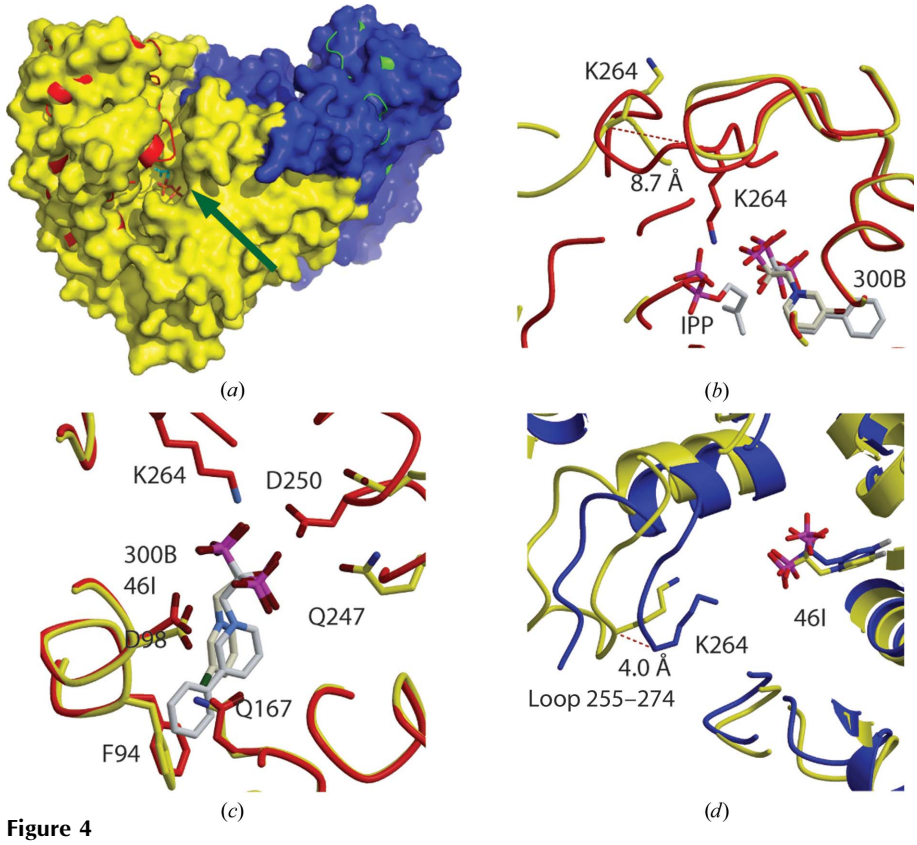

Figure 4
Structural comparisons of the active site of LmFPPS in complex with bisphosphonates in the presence and absence of IPP. (*a*) Surface representation of the complex with 46I and divalent cations (yellow and blue) overlapped with LmFPPS in complex with 300B, IPP and three divalent cations (red and green ribbon representation). The green arrow points to the cleft (opening) in the LmFPPS–46I–Mg complex in the absence of IPP. (*b*) Enlarged detail of (*a*) around the helix and the loop containing residues 255–274. The conserved residue Lys264 is observed to interact with the phosphate moiety of the allylic ligand (300B) in the closed conformation. In the LmFPPS–46I–Mg complex (yellow), in which the loop adopts the partially open conformation, Lys264 is 8.7 Å further away from corresponding residue that in the 300B complex (blue). (*c*) Structural overlap of LmFPPS in the complexes with 300B (red) and with 46I (yellow). Residues of the allylic site that have different conformations are shown. The inhibitor bound in each complex is shown. Metals are not shown for clarity. (*d*) Structural comparison of monomers *A* and *B* of LmFPPS in complex with 46I. In the region around the helix containing the second aspartate-rich motif and the loop 255–274, the conserved residue Lys264 is 4 Å further away from the allylic substrate in chain *B* than in chain *A*.

bind to this site in other FPPS structures (Rondeau *et al.*, 2006).

46I contains fluorine in the *meta* position of the phenyl group of the side chain (Fig. 3*d*, Supplementary Fig. S2). The interactions of the bisphosphonate moiety of 46I with protein residues are similar to those observed with the other two ligands, but there is additionally a hydrogen bond formed between the fluorine and Glu167. Unlike the other two structures, only two divalent cations (identified as Mg^{2+}) are found in the active site, coordinated by the conserved residues Asp98, Asp102 and Asp250 (Fig. 3*d*). Also, the residues Asp98 and Asp102 coordinating the comparable divalent ion in 300B complex are in a different conformation in the 46I complex owing to the missing divalent cation. Another difference involves the coordination of one of the ions (Ca^{2+} in the 300B complex and Mg^{2+} in the 46I complex). This ion shows a complete octahedral coordination in the 300B complex involving Asp250, water molecules and the allylic substrate 300B. In contrast, in the 46I complex the ion interacts with the ligand 46I indirectly through a water molecule.

3.4. Structural effects of IPP binding

The presence of IPP in the 300B structure, bound by residues Phe246, Arg108 and Lys264, introduces significant structural changes compared with the 46I complex. The loop that follows the second aspartate-rich region (residues 255–274) is in a different conformation in the two structures (Fig. 4*a*): it is displaced by up to 8.7 Å in the 46I complex (Fig. 4*b*). The closed conformation of the 300B complex is a direct result of the interactions of the protein with IPP. For example, closure of the loop owing to the presence of IPP brings Lys264 of the loop to interact directly with 300B (Fig. 4*b*).

3.5. Asymmetry in the LmFPPS–46I complex homodimers

The four monomers (*A*, *B*, *C* and *D*) in the asymmetric unit of the 46I complex crystal are organized into two dimers (*AB* and *CD*; r.m.s.d. of 0.56 Å), but within each dimer the monomers show significant differences (r.m.s.d. of 1.4 Å) localized in the loop containing residues 255–274. For example, residue Lys264 of monomer *A* is 5.6 Å away from the closest bisphosphonate O atom, but this residue is 8.0 Å away in monomer *B* (Fig. 4*d*). Another key difference between the chains of the LmFPPS–46I dimer is in the position of the Mg^{2+} ion coordinated to Asp250. In monomer *B* (or *D*), the helix containing the second aspartate-rich motif and the loop following this helix are in a more open conformation compared with chain *A* (or *C*). These changes create a large difference between the two monomers in the accessibility of the homoallylic site (see below).

We propose that the structure observed in the LmFPPS–46I–Mg complex represents a partially open intermediate structure which is ready for IPP to enter one of the two active sites, whereas the LmFPPS–300B–IPP–Ca and LmFPPS–476A–IPP–Ca complexes adopt the closed conformation after both the allylic and the homoallylic sites become occupied.

3.6. Comparisons of the LmFPPS and human FPPS (HsFPPS) structures

In both the human and *L. major* enzymes the divalent cations interact with the phosphates of the bisphosphonate, while IPP interacts with residues Lys48 and Arg108 of the enzyme. The residues involved in these interactions are conserved between the human and *L. major* proteins, as well as in FPPS from other species (Fig. 5*a*). This is also true for the residues at the bottom of the pocket, where bulky amino acids,

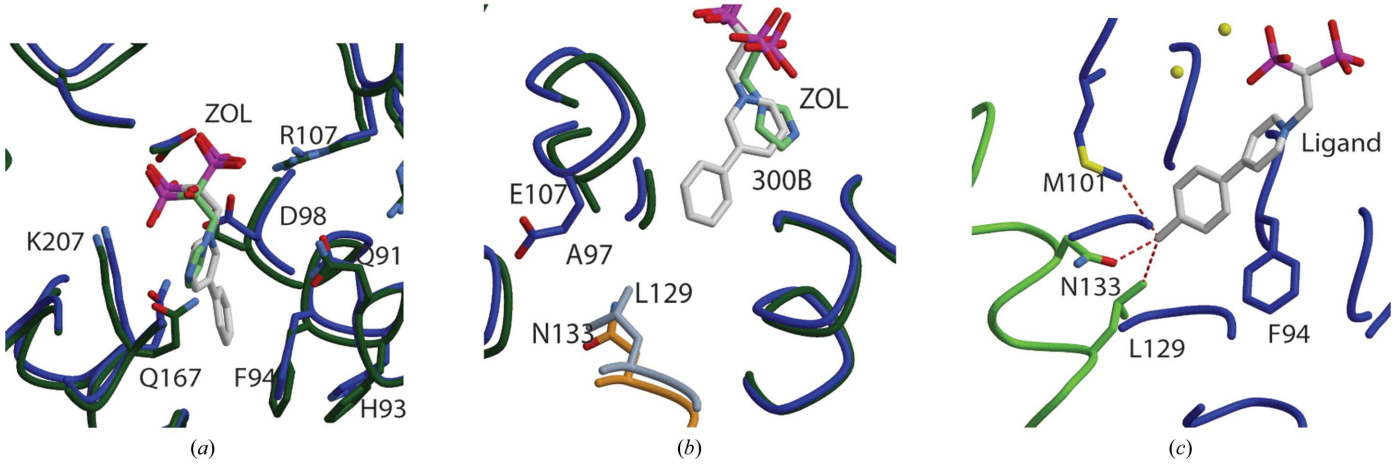

Figure 5
Structural comparisons between the active sites of LmFPPS and human FPPS. (*a*) LmFPPS in the 300B complex (blue) and HsFPPS in the zoledronate (Zol; 91B) complex (dark green) are shown in ribbon representation. While the conserved residues His93, Phe94, Asp98, Gln91 and Arg107 (stick models) are in the same conformation, Gln167 in 300B has a different conformation to accommodate the bulkier ligand. The ligands 300B (white) and Zol (light green) are shown as stick models. (*b*) Deeper in the allylic pocket two residues differ between the two molecules: Glu107 (dark blue, chain *A*) and Leu129 (light blue, chain *B*) of LmFPPS are replaced in HsFPPS by Ala97 (green, chain *A*) and Asn133 (orange, chain *B*). (*c*) The allylic site shown with a proposed inhibitor with a methyl group added to 300B. The relation of the methyl group to the nearest residues is shown by red dotted lines. The other monomer of the molecule is shown in green. Residues Leu129 and Asn133 from monomer *B* are shown as green stick models, while Met101 is shown as a blue stick model.

Phe94 and His93 in LmFPPS, restrict the length of the allylic product/substrate (Narita *et al.*, 1999; Szkopińska & Płochocka, 2005). In the region of the pocket that recognizes the isoprenoid chain, however, there are small but significant differences between the residues of HsFPPS and LmFPPS. For example, an alanine residue that points towards ligand at the bottom of the pocket of HsFPPS (Ala107) is replaced by a glutamate (Glu97) that points away from the ligand in LmFPPS, changing the shape of the pocket available for inhibitor binding. Another difference, the replacement of Leu129 in LmFPPS by Asn133 in HsFPPS at the bottom of the active site, can also potentially be exploited for the design of inhibitors that show specificity for the parasite enzyme (Fig. 5*b*). For example, a new inhibitor with a methyl added to the distal ring of 300B compound may exploit the differences between the human and *Leishmania* enzymes (Fig. 5*c*).

Table 2
Isothermal titration calorimetry studies on the binding of bisphosphonates to LmFPPS.

K_i values are reported from Sanders *et al.* (2005). ND, not determined.

Inhibitor	ΔG (kcal mol^{-1})	ΔH (kcal mol^{-1})	$-T\Delta S$ (kcal mol^{-1})	$1/K_a$ (nM)	LmFPPS K_i (nM)
91B	−10.4	3.15 ± 0.04	−13.6	28.0 ± 9.1	11
46I	−9.5	3.56 ± 0.05	−13.1	119.5 ± 23.4	50
300B	−8.9	4.42 ± 0.07	−13.3	342.5 ± 55.9	9
476A	−9.2	3.16 ± 0.07	−12.4	198.6 ± 57.8	ND

3.7. Entropy-driven ligand binding

The binding energetics of four inhibitors, 46I, 300B, 476A and 91B (zoledronate), to LmFPPS were measured using isothermal titration calorimetry (ITC). The data show that

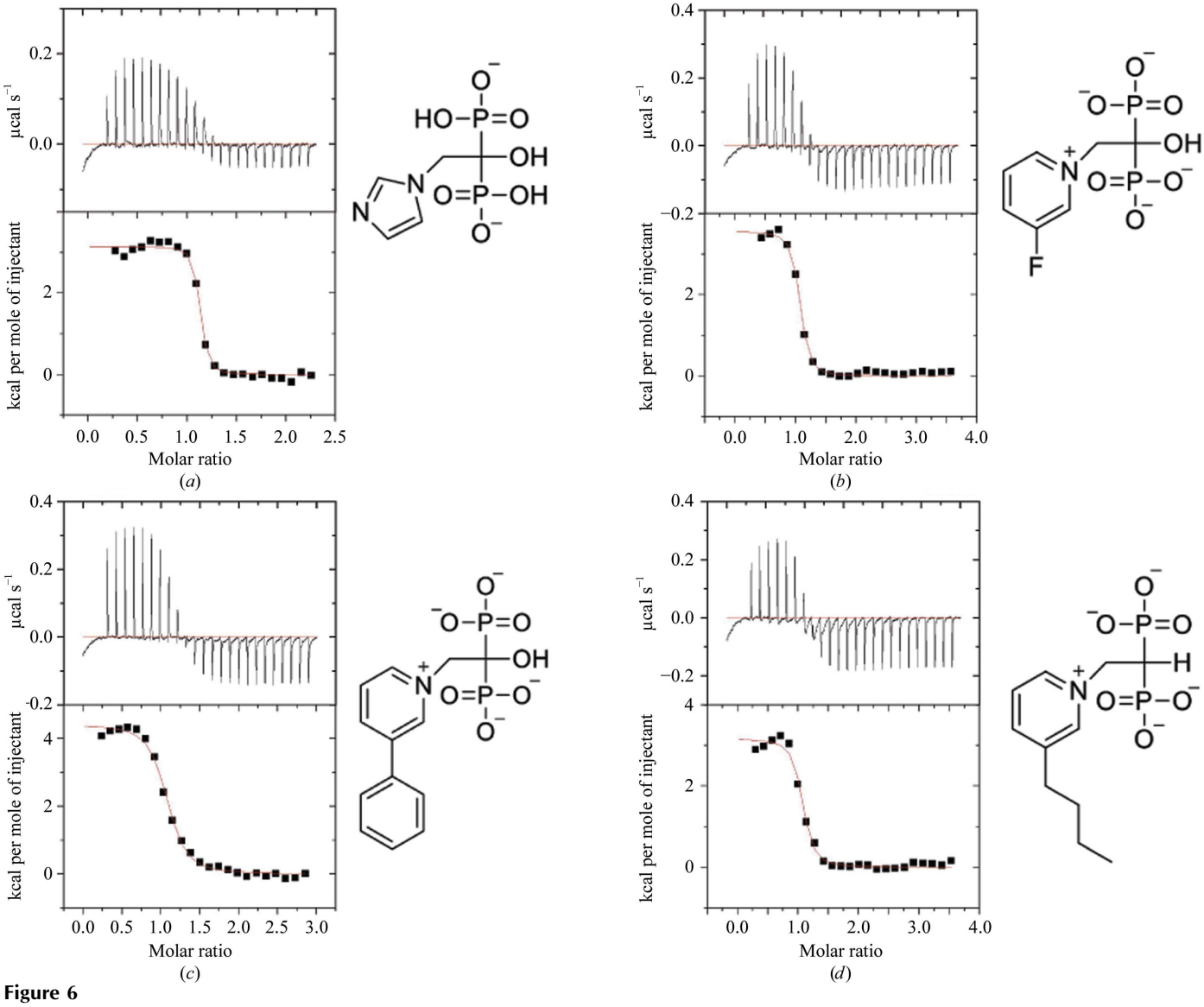

Figure 6
Thermodynamic analysis of LmFPPS binding. Isotherms for the binding of inhibitors 91B (*a*), 46I (*b*), 300B (*c*) and 476A (*d*) to LmFPPS. The top panels display the heat evolved for each injection and the bottom panels show the integrated heats of injection. The right panels show the chemical formulae. All of the curves are fitted to a one binding site per monomer model.

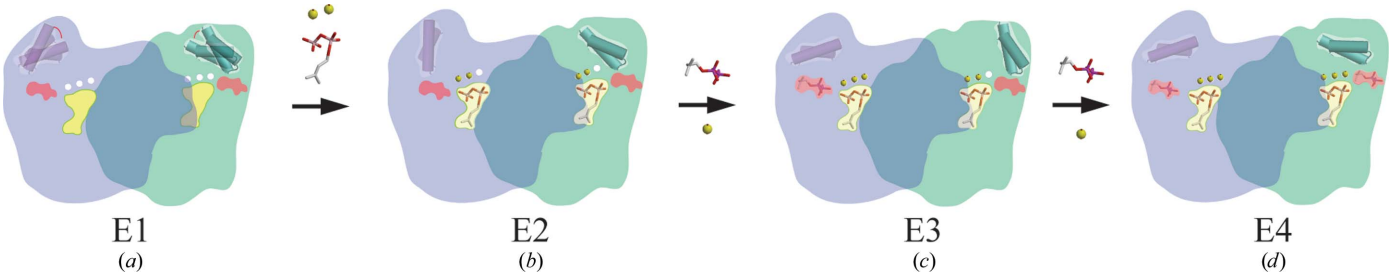

Figure 7
Mechanism of substrate binding to the LmFPPS dimer. Purple and green shaded regions correspond to the two monomers of the FPPS homodimer. In each monomer, the allylic site is shown as a yellow shaded region and the homoallylic site is shown in red. Blue spheres represent empty divalent cation sites, while the yellow spheres represent occupied cation sites. The loop 255–274 is shown as either purple or green cylinders. (*a*) Apo structure (E1) with none of the sites occupied and in which the conformation of the loop can be either open or closed. The movement of the loop is indicated by a red curve. (*b*) Partially open form (E2) in which DMAPP and two divalent cations occupy the allylic sites of each monomer. The loop 255–274 is in a more open conformation in one monomer (purple cylinder) than in the other monomer (green cylinder). This partially open conformation corresponds to that of the LmFPPS–46I–Mg complex. (*c*) The asymmetry of the conformations of the loop in the two monomers (E3) suggests that IPP and a third divalent cation bind to one of the monomers, causing a conformational change priming for the entry of the second IPP molecule. (*d*) Closed form (E4) as observed in the LmFPPS–300B–IPP–Ca and LmFPPS–476A–IPP–Ca complexes, in which the allylic site, the homoallylic site and the three divalent cation sites are fully occupied and the residues in the loop 255–274 are in the closed conformation.

in all cases binding is entropy-driven. The reactions are endothermic ($\Delta H > 0$; Table 2, Fig. 6), with K_d values in the range 28.0–342.5 n*M*. The entropies of binding are in the range 41.2–45.2 cal K^{-1} mol^{-1} ($-T\Delta S$ is between −12.4 and −13.6 kcal mol^{-1}), similar to those reported previously for other cationic side-chain-containing bisphosphonates binding to *T. brucei* FPPS (Montalvetti *et al.*, 2003). The smaller ligands 46I and 91B bind more tightly than the larger ligands 300B and 476A. Also, 91B binds fivefold less tightly, with a K_d of 150 n*M*, to HsFPPS than to LmFPPS (Kavanagh *et al.*, 2006). In the case of 300B, the reduced affinity results from a binding enthalpy that is more unfavourable than those of the other inhibitors. This may be a consequence of the increased difficulty in accommodating this larger compound within the binding site. Interestingly, the entropic contribution to the binding of 300B is more favourable than that to the binding of 476A. This is probably owing to the combination of two opposing effects: (i) a loss of conformational entropy owing to freezing of single bonds in the bisphosphonate, more so in 476A (it has more rotatable single bonds) than in 300B, and (ii) the larger hydrophobic surface of 300B, resulting in a release of larger number of water molecules organized around its side chain. Even though smaller ligands bind more tightly to the protein, 300B has the best inhibitory efficacy against the activity of the enzyme. The inhibition data (IC_{50}) of 91B and 46I are in agreement with the K_d values obtained by ITC (Table 2). These results, together with the structural data, suggest that inhibition results from binding of the inhibitor to the allylic site of the enzyme. Comparison of the binding affinities of LmFPPS with those previously determined for HsFPPS (K_d of 28 n*M* for LmFPPS *versus* 150 n*M* for HsFPPS shows a small window of improvement that can be capitalized on.

3.8. Mechanistic insights

Before this work, the coordinates of 55 complexes of FPPS from diverse species had been deposited in the PDB. None of these had only the homoallylic site occupied, probably indicating that the allylic substrate binds first to the dimer. Reinforcing this hypothesis, the structure of the LmFPPS dimer complex with 46I has the allylic sites occupied while the homoallylic sites are empty. Notably, it is only in the 46I complex that the dimers are not symmetrical: in each dimer, the homoallylic site of one of the monomers is significantly more open than that of the other monomer. The differences are mainly localized in the loop spanning residues 255–274 (Figs. 3*b* and 7). The open monomers (*B* and *D*) provide a clear path for the IPP substrate to reach its binding site. In contrast, the other monomers (*A* and *C*) would require changes in their structures in order to allow IPP to reach its binding site. The structures of the GgFPPS–DMAP and GgFPPS–GPP complexes (PDB entries 1ubw and 1uby) in the absence of IPP have a conformation similar to the 'open' conformation observed in LmFPPS–46I, strengthening the argument that this conformation exists and is relevant for the natural substrates (Tarshis *et al.*, 1996). This observation provides structural insight into the ordered binding proposed by Laskovics & Poulter (1981): both allylic sites are occupied first, resulting in an asymmetric structure with one of the monomers in a conformation ideally suited to accept IPP. Binding of IPP to this monomer results in a conformational change that opens the homoallylic site of the other monomer, which closes after binding the second IPP (Laskovics & Poulter, 1981). These changes would result in the symmetric dimer observed in all previous complexes with both allylic and homoallylic sites occupied.

This work was supported by National Institutes of Health grants GM065307 and CA158191 to EO and in part by the Plan Nacional SAF2010-20059 to DGP. Use of the Advanced Photon Source at Argonne National Laboratory was supported by the United States Department of Energy under contract DE-AC0206CH11357. Use of the Lilly Research Laboratory collaborative access team LRL-CAT beamline at

sector 31 of the Advanced Photon Source was provided by Eli Lilly Co., who operate the facility.

References

Emsley, P., Lohkamp, B., Scott, W. G. & Cowtan, K. (2010). *Acta Cryst.* D**66**, 486–501.

Gabelli, S. B., McLellan, J. S., Montalvetti, A., Oldfield, E., Docampo, R. & Amzel, L. M. (2006). *Proteins*, **62**, 80–88.

Hooft, R. W. W., Sander, C. & Vriend, G. (1996). *J. Appl. Cryst.* **29**, 714–716.

Hooft, R. W. W., Vriend, G., Sander, C. & Abola, E. E. (1996). *Nature (London)*, **381**, 272.

Huang, C.-H., Gabelli, S. B., Oldfield, E. & Amzel, L. M. (2010). *Proteins*, **78**, 888–899.

Jancarik, J. & Kim, S.-H. (1991). *J. Appl. Cryst.* **24**, 409–411.

Jones, T. A., Zou, J.-Y., Cowan, S. W. & Kjeldgaard, M. (1991). *Acta Cryst.* A**47**, 110–119.

Kavanagh, K. L., Guo, K., Dunford, J. E., Wu, X., Knapp, S., Ebetino, F. H., Rogers, M. J., Russell, R. G. & Oppermann, U. (2006). *Proc. Natl Acad. Sci. USA*, **103**, 7829–7834.

Kraulis, P. J. (1991). *J. Appl. Cryst.* **24**, 946–950.

Laskovics, F. M. & Poulter, C. D. (1981). *Biochemistry*, **20**, 1893–1901.

Laskowski, R. A., MacArthur, M. W., Moss, D. S. & Thornton, J. M. (1993). *J. Appl. Cryst.* **26**, 283–291.

Lee, B. & Richards, F. M. (1971). *J. Mol. Biol.* **55**, 379–400.

Montalvetti, A., Fernandez, A., Sanders, J. M., Ghosh, S., Van Brussel, E., Oldfield, E. & Docampo, R. (2003). *J. Biol. Chem.* **278**, 17075–17083.

Murshudov, G. N., Skubák, P., Lebedev, A. A., Pannu, N. S., Steiner, R. A., Nicholls, R. A., Winn, M. D., Long, F. & Vagin, A. A. (2011). *Acta Cryst.* D**67**, 355–367.

Narita, K., Ohnuma, S. & Nishino, T. (1999). *J. Biochem.* **126**, 566–571.

Navaza, J. (1994). *Acta Cryst.* A**50**, 157–163.

Ohnuma, S., Narita, K., Nakazawa, T., Ishida, C., Takeuchi, Y., Ohto, C. & Nishino, T. (1996). *J. Biol. Chem.* **271**, 30748–30754.

Ortiz-Gómez, A., Jiménez, C., Estévez, A. M., Carrero-Lérida, J., Ruiz-Pérez, L. M. & González-Pacanowska, D. (2006). *Eukaryot. Cell*, **5**, 1057–1064.

Otwinowski, Z. & Minor, W. (1997). *Methods Enzymol.* **276**, 307–326.

Reszka, A. A., Halasy-Nagy, J. M., Masarachia, P. J. & Rodan, G. A. (1999). *J. Biol. Chem.* **274**, 34967–34973.

Rodan, G. A. & Martin, T. J. (2000). *Science*, **289**, 1508–1514.

Rodriguez, N., Bailey, B. N., Martin, M. B., Oldfield, E., Urbina, J. A. & Docampo, R. (2002). *J. Infect. Dis.* **186**, 138–140.

Rondeau, J. M., Bitsch, F., Bourgier, E., Geiser, M., Hemmig, R., Kroemer, M., Lehmann, S., Ramage, P., Rieffel, S., Strauss, A., Green, J. R. & Jahnke, W. (2006). *ChemMedChem*, **1**, 267–273.

Sanders, J. M. *et al.* (2005). *J. Med. Chem.* **48**, 2957–2963.

Szkopińska, A. & Płochocka, D. (2005). *Acta Biochim. Pol.* **52**, 45–55.

Tarshis, L. C., Proteau, P. J., Kellogg, B. A., Sacchettini, J. C. & Poulter, C. D. (1996). *Proc. Natl Acad. Sci. USA*, **93**, 15018–15023.

Tarshis, L. C., Yan, M., Poulter, C. D. & Sacchettini, J. C. (1994). *Biochemistry*, **33**, 10871–10877.

Winn, M. D. *et al.* (2011). *Acta Cryst.* D**67**, 235–242.

Winn, M. D., Isupov, M. N. & Murshudov, G. N. (2001). *Acta Cryst.* D**57**, 122–133.

World Health Organization (2014). *Leishmaniasis*. http://www.who.int/leishmaniasis/en/. Geneva: World Health Organization.

Zhang, Y., Leon, A., Song, Y., Studer, D., Haase, C., Koscielski, L. A. & Oldfield, E. (2006). *J. Med. Chem.* **49**, 5804–5814.